Specialized neurons in the right habenula mediate response to aversive olfactory cues

Jung-Hwa Choi[1,3], Erik Duboué[2], Michelle Macurak[1], Jean-Michael Chanchu[1] and Marnie E. Halpern[1,3,*]

1. Carnegie Institution for Science, Department of Embryology, Baltimore, Maryland, 21218, USA
2. Jupiter Life Science Initiative, Florida Atlantic University, Jupiter, FL 33458, USA; Wilkes Honors College, Florida Atlantic University, Jupiter, FL 33458, USA
3. Current address: Geisel School of Medicine at Dartmouth, Department of Molecular and Systems Biology, 725 Remsen, Hanover, NH 03755, USA

*Author for correspondence Marnie.E.Halpern@dartmouth.edu

Abstract

Hemispheric specializations are well studied at the functional level but less is known about the underlying neural mechanisms. We identified a small cluster of cholinergic neurons in the right dorsal habenula (dHb) of zebrafish, defined by their expression of the *lecithin retinol acyltransferase domain containing 2a* (*lratd2a*) gene and their efferent connections with a subregion of the ventral interpeduncular nucleus (vIPN). The unilateral *lratd2a*-expressing neurons are innervated by a subset of mitral cells from both the left and right olfactory bulb and are activated upon exposure of adult zebrafish to the aversive odorant cadaverine that provokes avoidance behavior. Using an intersectional strategy to drive expression of the botulinum neurotoxin specifically in these neurons, we find that adults no longer show protracted avoidance to cadaverine. Mutants with left-isomerized dHb that lack these neurons are less repelled by cadaverine and their behavioral response to alarm substance, a potent aversive cue, is diminished. However mutants in which both dHb have right identity appear more reactive to alarm substance. The results implicate an asymmetric dHb-vIPN neural circuit in processing of aversive olfactory cues and modulating resultant behavioral responses.

Introduction

Fish use the sense of smell to search for food, detect danger, navigate and communicate social information by detecting chemical cues in their aquatic environment (Yoshihara, 2014). As with birds and mammals, perception of olfactory cues is lateralized and influences behavior (Siniscalchi, 2017). In zebrafish, nine glomerular clusters in the olfactory bulb (OB) receive olfactory information from sensory neurons in the olfactory epithelium and, in turn, transmit signals to four forebrain regions: the posterior zone of the dorsal telencephalon (Dp), the ventral nucleus of the ventral telencephalon (Vv), the posterior tuberculum (PT), and the dorsal habenular region (dHb) (Miyasaka et al., 2014; Yoshihara, 2014). In contrast to all other target regions that are located on both sides of the forebrain, only the right nucleus of the dHb is innervated by mitral cells that emanate from medio-dorsal (mdG) and ventro-medial (vmG) glomerular clusters in both OBs (Miyasaka *et al.*, 2014; Yoshihara, 2014). Moreover, calcium imaging experiments suggest that the right dHb shows a preferential response to odorants compared to the left dHb (Chen et al., 2019; Dreosti et al., 2014; Jetti et al., 2014; Krishnan et al., 2014). The identity of the post-synaptic neurons within the right dHb that receive olfactory input and the purpose of this asymmetric connection are unknown.

The habenulae are highly conserved structures in the vertebrate brain and, in teleosts such as zebrafish, consist of dorsal and ventral (vHb) nuclei, which are equivalent to the medial and lateral habenulae of mammals, respectively (Amo et al., 2010). The neurons of the dHb are largely glutamatergic and contain specialized subpopulations that also produce acetylcholine, substance P or somatostatin. In zebrafish, the number of neurons within each subtype differs between the left and right dHb (deCarvalho et al., 2014; Hsu et al., 2016). The dHb have been implicated in diverse states such as reward, fear, anxiety, sleep and addiction (Duboué et al., 2017; Hikosaka, 2010;

Okamoto et al., 2012). Accordingly, the right dHb was shown to respond to bile acid and involved in food-seeking behaviors (Chen *et al.*, 2019; Krishnan *et al.*, 2014), whereas the left dHb was found to be activated by light and attenuate fear responses (Dreosti *et al.*, 2014; Facchin et al., 2015; Zhang et al., 2017). However, the properties of the dHb neurons implicated in these behaviors, such as their neurotransmitter identity and precise connectivity with their unpaired target, the midbrain interpeduncular nucleus (IPN), have yet to be determined.

Here, we describe a group of cholinergic neurons defined by their expression of the *lecithin retinol acyltransferase domain containing 2a* (*lratd2a*) gene [formerly known as *family with sequence similarity 84 member B* (*fam84b*)], that are located in the right dHb where they are selectively innervated by the olfactory mitral cells that originate from both sides of the brain (Miyasaka et al., 2009), and form efferent connections with a restricted subregion of the ventral IPN (vIPN). Activity of the *lratd2a*-expressing neurons is increased following exposure to the aversive odorant cadaverine and their inactivation alters the avoidance behavior of adult zebrafish to this repulsive cue. Our findings provide further evidence for functional specialization of the left and right habenular nuclei and reveal the neuronal pathway that mediates a lateralized olfactory response.

Materials and Methods

Zebrafish

Zebrafish were maintained at 27 °C in a 14:10 h light/dark cycle in a recirculating system with dechlorinated water (system water). The AB wild-type strain (Walker, 1998), transgenic lines *Tg(lratd2a:QF2)*^{c601}, *Tg(slc5a7a:Cre)*^{c662}, *Tg(Xla.Tubb2:QF2;he1.1:mCherry)*^{c663}, *Tg(QUAS:GCaMP6f)*^{c587}, *Tg(QUAS:BoTxBLC-GFP)*^{c605}, *Tg(QUAS:mApple-CAAX;he1.1:mCherry)*^{c636}, *Tg(QUAS:loxP-mCherry-loxP-GFP-CAAX)*^{c679}, and *Tg(QUAS:loxP-mCherry-loxP-BoTxBLC-GFP)*^{c674}, *Tg(-10lhx2a:gap-EYFP)*^{zf177} (formally known as *Tg(lhx2a:gap-YFP)*) (Miyasaka *et al.*, 2009), and mutant strains *tcf7l2*^{zf55} (Muncan et al., 2007) and *bsx*^{m1376} (Schredelseker and Driever, 2018) were used. For imaging, embryos and larvae were transferred to system water containing 0.003% phenylthiourea (PTU) to inhibit melanin pigmentation. All zebrafish protocols were approved by the Institutional Animal Care and Use Committee (IACUC) of the Carnegie Institution for Science or Dartmouth College.

Generation of transgenic lines by *Tol2* transgenesis

The MultiSite Gateway-based construction kit (Kwan et al., 2007) was used to create transgenic constructs for Tol2 transposition. A 16 bp *QUAS* sequence (Potter et al., 2010), was cloned into the 5' entry vector (*pDONRP4-P1R*, #219 of Tol2kit v1.2) via a BP reaction (11789020, Thermo Fisher Scientific). Middle entry vectors (*pDONR221*, #218 of Tol2kit v1.2 (Kwan *et al.*, 2007)) were generated for *QF2*, *mApple-CAAX*, *loxP-mCherry-stop-loxP*, *GCaMP6f* and *BoTxBLC-GFP*. Sequences corresponding to the *SV40 poly A* tail, the *SV40 poly A* tail followed by a secondary marker consisting of the zebrafish *hatching enzyme 1* promoter (Xie et al., 2012) driving mCherry,

or to *BoTxBLC-GFP* (Lal et al., 2018; Sternberg et al., 2016; Zhang *et al.*, 2017) were cloned into the 3' entry vector (*pDONRP2R-P3*, #220 of Tol2kit v1.2 (Kwan *et al.*, 2007)). Final constructs were created using an LR reaction (11791020, Thermo Fisher Scientific) into a Tol2 destination vector (*pDestTol2pA2*, #394 of the Tol2kit v1.2 (Kwan *et al.*, 2007)) (Supplementary table 1).

To produce Tol2 transposase mRNA, *pCS-zT2TP* was digested by *Not*I and RNA synthesized using the mMESSAGE mMACHINE SP6 Transcription Kit (AM1340, Thermo Fisher Scientific). RNA was purified by phenol/chloroform-isoamyl extraction, followed by chloroform extraction and isopropanol precipitation (Suster et al., 2011). A solution containing *QF2/QUAS* plasmid DNA (~25 ng/µl), transposase mRNA (~25 ng/µl) and phenol red (0.5%) was microinjected into one-cell stage zebrafish embryos, which were raised to adulthood. To identify transgenic founders, F_0 adult fish were outcrossed to AB and embryos were assessed for the presence of the secondary marker by screening for mCherry labeling of hatching gland cells after 24 hpf and raised to adulthood.

Generation of transgenic lines by genome editing

For generating transgenic lines at targeted sites, we performed CRISPR/Cas9-mediated genome editing using the method of Kimura *et al*. (Kimura et al., 2014), which relies on homology-independent repair of double-strand breaks for integration of donor DNA. To construct the donor DNA, we combined GFP bait sequences (Gbait) and the hsp70 promoter fragment (Kimura *et al.*, 2014), with a QF2 sequence, which contains the DNA binding and transcriptional activation domains of the QF transcription factor of *Neurospora crassa* (Ghosh and Halpern, 2016; Subedi et al., 2014). The Gbait-hsp70 sequence was amplified with forward 5'-GGCGAGGGCGATGCCACCTACGG-3' and reverse 5'-

CCGCGGCAAGAAACTGCAATAAAAAAAAC-3' primers, using Gbait-hsp70:Gal4 donor DNA (Kimura *et al.*, 2014). QF2 sequence was amplified with forward 5'-ACTAGTATGCCACCCAAGCGCAAAACGC-3' and reverse 5'-CTGCAGCAACTATGTATAATAAAGTTGAAA-3' primers, using pDEST:QF2 template DNA Subsequently, the Gbait-hsp70 fragment and QF2 fragment were independently inserted into pGEM T-easy (A1360, Promega) and subsequently combined into one vector by *Sac*II digestion and ligation (Addgene, plasmid #122563). The Cre sequence was amplified using pCR8GW-Cre-pA-FRT-kan-FRT as template DNA (Suster *et al.*, 2011) and (forward 5'-ACTAGTGCCACCATGGCCAATTTACTG-3', and reverse 5'-CTGCAGGGACAAACCACAACTAGA-3') primers, and inserted into pGEM T-easy. The Gbait-hsp70 fragment was subcloned into the Cre vector by *Sac*II digestion and ligation (Addgene, plasmid #122562).

Production of sgRNAs and Cas9 RNA was performed as described previously (Hwang et al., 2013; Jao et al., 2013). Potential sgRNAs were designed using Zifit (Sander et al., 2010). Pairs of synthetic oligonucleotides (*lratd2a* sense, 5'-TAGGACTGGACACCGAAGAAGA-3'; *lratd2a* anti-sense, 5'-AAACTCTTCTTCGGTGTCCAGT-3'; *slc5a7a* sense, 5'-TAGGCTCTTTGTGCACTGTTGG-3'; *slc5a7a* anti-sense, 5'-AAACCCAACAGTGCACAAAGAG-3'), 5'-TAGG-N_{18}-3' and 5'-AAAC-N_{18}-3', were annealed and inserted at the *Bsa*I site of the pDR274 vector (Addgene, plasmid #42250). To make sgRNA and Cas9 mRNA, template DNA for sgRNAs and pT3TS nCas9n (Addgene, plasmid #46757) were digested by *Dra*I and *Xba*I, respectively. The MAXIscript T7 Transcription Kit (AM1312, Thermo Fisher Scientific) was used for synthesis of sgRNAs from linearized DNA template and the mMESSAGE mMACHINE T3 Transcription Kit (AM1348, Thermo Fisher

Scientific) for synthesis of Cas9 RNA. RNA was purified by phenol/chloroform and precipitated by isopropanol.

A solution containing sgRNA for the targeted gene (~50 ng/µl), sgRNA (~50 ng/µl) to linearize donor plasmids at the Gbait site (Auer et al., 2014; Kimura *et al.*, 2014), the Gbait-hsp70-QF2-pA and Gbait-hsp70-Cre-pA (~50 ng/µl) plasmids, Cas9 mRNA (~500 ng/µl), and phenol red (0.5%) was microinjected into one-cell stage embryos. To verify integration of donor DNA at the target locus, PCR was performed using primers that correspond to sequences flanking the integration site and within the donor plasmid (*hsp70* reverse, 5'-TCAAGTCGCTTCTCTTCGGT-3'). (For *lratd2a, the* forward primer is 5'-CTGCTGAAGTGGCATTTATGGGC-3' and the reverse primer is 5'-CCTGGAAGTCCCCGACATAC-3'; for *slc5a7a* the forward primer is 5'-CACATCTCTCTGACGTCCATC-3' and the reverse is 5'-GTTGCTGCGCAGGACTTAAAA-3'). Sequence analysis of PCR products confirmed integration at the targeted sites.

RNA *in situ* hybridization

Whole-mount *in situ* hybridization was performed as previously described (deCarvalho *et al.*, 2014; Gamse et al., 2002). In brief, larvae and dissected brains were fixed in 4% paraformaldehyde (P6148, Sigma-Aldrich) in 1X PBS (phosphate-buffered saline) at 4 °C overnight. To synthesize RNA probes, the following restriction enzymes and RNA polymerases were used: *lratd2a* (*Bam*HI/T7), *fos* (*Not*I/SP6), *slc5a7a* (*Not*I/SP6), *kctd12.1* (*Eco*RI/T7) (deCarvalho et al., 2013; Hong et al., 2013). Probes were labeled with UTP-digoxigenin (11093274910, Roche) and samples incubated at 70 °C in hybridization solution containing 50% formamide. Hybridized probes were detected using alkaline phosphatase-conjugated antibodies (Anti-Digoxigenin-AP, #11093274910, and Anti-Fluorescein-AP, #11426338910, Sigma-Aldrich) and visualized by

staining with 4-nitro blue tetrazolium (NBT, #11383213001, Roche), 5-bromo-4-chloro-3-indolyl-phosphate (BCIP, #11383221001, Roche) and 2-(4-Iodophenyl)-3-(4-nitrophenyl)-5-phenyltetrazolium Chloride (INT, #I00671G, Fisher Scientific).

Preparation of odorants

Alarm substance was freshly prepared on the day of testing. Adult zebrafish (6 female and 6 male) were anesthetized in 0.02% tricaine (E10521, Ethyl 3-aminobenzoate methanesulfonate; Sigma-Aldrich). Shallow lesions were made on the skin (10 on each side) using a fresh razor blade and single fish were consecutively immersed in a beaker containing distilled water (25 ml for *fos* experiment and 50 ml for behavioral analyses) for 30 seconds at 4 °C. The solution was filtered using a 0.2 µm filter (565-0020, ThermoFisher Scientific) and stored at 4 °C until used (Mathuru et al., 2012). The cadaverine (#33211, final concentration 100 µM) and chondroitin sulfate (#c4384, 100 µg/ml) were purchased from Sigma-Aldrich, and stock solutions prepared in distilled water.

Calcium imaging in larval and juvenile zebrafish

Calcium imaging was performed on 7, 14 and 21-22 dpf *Tg(lratd2a:QF2)*^{c644}; *Tg(QUAS:GCaMP6f)*^{c587} individuals. Larvae and juveniles were paralyzed by immersion in α-bungarotoxin (20 µl of 1 mg/ml solution in system water, B1601, ThermoFisher Scientific) (Duboué *et al.*, 2017; Severi et al., 2014) followed by washing in fresh system water. Individual fish were embedded in 2% low melting agarose in a petri dish (60 mm) with a custom-designed mold. After solidification, the agarose around the nose was carefully removed with forceps for access to odorants, and the individual immersed in fresh system water. The dish was placed under

a 25X (NA = 0.95), on a Leica SP5 (for chondroitin sulfate) or under a 20X (NA=0.5) water immersion objective on a Zeiss LSM 980 (for cadaverine) confocal microscope. Images were acquired in *XYZT* acquisition mode at 512 X 200 pixel resolution at a rate of 2 Hz and digitized 8 bit from two focal planes. To calculate fluorescence intensity, regions of interest (ROI) were manually drawn around each cell in the average focal plane with the polygon tool and ROI *manage* in Fiji (Schindelin et al., 2012). To normalize calcium activity for each cell to baseline fluorescence (average of 250 frames from each neuron), the fractional change in fluorescence ($\Delta F/F$) was calculated before the application of odorants, according to the formula $F = (F_i-F_0)/F_0$, where F_i is the fluorescence intensity at a single time point and F_0 is the baseline fluorescence. All data and images were analyzed using custom programs in MATLAB (MathWorks, version 7.3) and Excel software.

Assay of *fos* expression in adult zebrafish

Individual adult zebrafish (7–9 months old) were placed in a tank with 1 L system water and acclimated for at least 1 hour prior to odorant exposure. Each odorant solution (1 ml) was gently pipetted into the tank water and the fish was kept there as the odorant diffused. After 30 min, the fish was sacrificed in an ice water slurry, and the brain dissected out and fixed in 4% paraformaldehyde in 1X PBS overnight at 4 °C. Fixed brains were embedded in 4% low melting agarose (SeaPlaque® Agarose, Lonza) in 1X PBS and sectioned at 50 µm (for juvenile brains) or 70 µm (for adult brains) using a vibratome (VT1000S, Leica Biosystems, Inc.). For more precise counting of *fos* expressing cells in adult brains, habenular sections were 35 µm thick. Sections were covered in 50% glycerol in 1X PBS under coverslips. Bright-field images were captured with a Zeiss AxioCam HRc camera mounted on a Zeiss Axioskop. A Leica SP5 confocal microscope

215 was used for fluorescent images. Data from *fos* RNA *in situ* hybridization experiments were
216 quantified using ImageJ/Fiji software (Schindelin *et al.*, 2012).
217
218 Behavioral assays
219 Behavioral assays were performed using 5 – 7 week old juvenile zebrafish and adults between 4
220 and 8 months of age. Responses to odorants were measured between 10:00 a.m. and 4:00 p.m. and
221 fish were starved for 1 day prior to testing (Koide et al., 2009). Individual adults were placed in a
222 1.5 L test tank (Aquatic Habitats) in 1 L of system water and allowed to acclimate for at least 1
223 hour. For experiments with juveniles, individuals were acclimated to the behavior room for 1 hour,
224 gently netted into the test tank (20 x 9 x 8.3 cm, 1.5 L mating cage) with 0.6 L system water and
225 maintained there for 5 min prior to testing. Swimming activity was recorded for 5 min (4 min for
226 juveniles) before and after the application of odorants. Odorants (2 ml for adults, 1 ml for juveniles)
227 were slowly expelled through plastic tubing (Tygon R-3606; 0.8 mm ID, 2.4 mm OD) attached on
228 one end to a 3 ml syringe (BD 309657) and on the other positioned at one end of the test tank.
229 Preference indices were calculated using the formula: preference to odorants = (Total time spent
230 in the tank half where odorant was delivered) – (Total time spent in the other half of the tank)/Total
231 time (Koide *et al.*, 2009; Wakisaka et al., 2017).
232
233 Quantification and statistical analyses
234 Analyses were performed using custom written scripts in MATLAB (The MathWorks). Mann
235 Whitney *U* and Student's *t* tests were used to compare nonparametric unmatched groups. One-
236 sample *t* test against 0 was used for analyzing the preference to cadaverine. The significance was

two-tailed for all tests and depicted as n.s. (non-significant, $P > 0.05$) or with significance as *$P<0.05$, **$P<0.01$, ***$P<0.001$, and ****$P<0.0001$.

Results

lratd2a-expressing neurons in the right dHb receive bilateral olfactory input

A subset of medio-dorsal mitral cells that are labeled by *Tg(lhx2a:gap-YFP)* were previously shown to project their axons bilaterally through the telencephalon and terminate in the right dHb (Miyasaka *et al.*, 2009), in the vicinity of a small population of *lratd2a*-expressing neurons [(deCarvalho *et al.*, 2013) and Figure 1A]. To characterize this subset of right dHb neurons, we used CRISPR/Cas9-mediated targeted integration (Kimura *et al.*, 2014) to introduce the QF2 transcription factor (Ghosh and Halpern, 2016; Subedi *et al.*, 2014) under the control of *lratd2a* regulatory sequences (Figure 1B). QF2 does not disrupt transcription at the *lratd2a* locus (Supplementary figure 1) and drives expression of QUAS regulated fluorescent reporter genes in a similar pattern as endogenous gene expression in the nervous system (deCarvalho *et al.*, 2013). In 4 dpf larval zebrafish, this includes a subset of neurons in the OB, the bilateral vHb, and a small cluster of neurons in the right dHb (Figures 1C-E''). Double labeling confirms that the axons of *lhx2a* olfactory neurons terminate precisely at the *lratd2a*-expressing right habenular neurons (Figures 1C-D''), which project to a restricted region of the ventral IPN (Figures 1F-G'').

Aversive olfactory cues activate *lratd2a* neurons in the right dHb

Several studies using transgenic expression of the genetically encoded calcium indicator GCaMP have demonstrated that dHb neurons respond to olfactory cues in larval zebrafish (Jetti *et al.*, 2014; Krishnan *et al.*, 2014). To determine whether olfactants activate the *lratd2a* positive neuronal cluster in the right dHb, we analyzed calcium signaling in *Tg(lratd2a:QF2)*^{c644}, *Tg(QUAS:GCaMP6f)*^{c587} larval and juvenile zebrafish. Following exposure of 7, 14 and 21 dpf individuals to cadaverine (Figures 2A-B, Supplementary figures 2 and 3), a known aversive

olfactory cue that is released from decaying fish (Hussain et al., 2013), we measured a two-fold increase in activity compared to that after application of water alone. The *lratd2a* dHb neurons also responded to chondroitin sulfate, a component of alarm substance (also known as Schreckstoff), which is released from the skin of injured fish (Mathuru *et al.*, 2012). A two-fold increase in calcium signals was detected after the first and second delivery of chondroitin sulfate to 22 dpf larvae and a four-fold increase after the second application to 7 and 14 dpf larvae (Figures 2A-B, Supplementary figures 2 and 3).

To examine whether the response to aversive odorants persists in the olfactory-dHb pathway of adult zebrafish, we used expression of the *fos* gene as an indicator of neuronal activation (deCarvalho *et al.*, 2013; Hong *et al.*, 2013). Consistent with previous findings (Dieris et al., 2017), cadaverine broadly activated OB mitral neurons in the dorsal glomerulus (dG), dorso-lateral glomerulus (dlG), medio-anterior glomerulus (maG), medio-dorsal glomerulus (mdG), lateral glomerulus (lG). In addition, we observed a 3-fold increase in the number of *fos*-expressing neurons in the right dHb following exposure of adult zebrafish to cadaverine relative to delivery of water alone (15.73 ± 1.25 vs. 5.61 ± 1.07 cells, Figures 2C-D). The position of the *fos*-expressing cells in the right dHb corresponds to that of the *lratd2a*-expressing neurons (Figure 2C). Thus, the *lratd2a* subpopulation in the right dHb responds to cadaverine in both larvae and adults.

Exposure to alarm substance prepared from adult zebrafish increased the number of *fos*-expressing mitral cells not only in the lateral glomerulus (lG) and dlG of the OB as would be expected (Mathuru *et al.*, 2012; Yoshihara, 2014), but also in the dorso-lateral region of the dHb (Figures 2C-D). In contrast to cadaverine, alarm substance activated neurons in both the left and right dHb (20.72 ± 2.70 cells on the left and 20.31 ± 2.53 on the right).

Synaptic inhibition of right dHb *lratd2a* neurons reduces aversive response to cadaverine

To confirm that *lratd2a* expressing neurons play a role in processing of aversive olfactory cues, we inhibited synaptic transmission in these cells by mating *Tg(lratd2a:QF2)* fish to a newly generated transgenic line, *Tg(QUAS:BoTxBLC-GFP)*^{c605}, in which Botulinum toxin light chain C (*BoTxBLC*) (Lal *et al.*, 2018; Sternberg *et al.*, 2016; Zhang *et al.*, 2017) is placed under QUAS control. We tested how adults from the *BoTxBLC-GFP* line reacted to cadaverine by introducing the odorant to one end of a test tank, and measuring the time individuals spent within or outside of this region of the tank. Adults bearing *Tg(lratd2a:QF2)* and *Tg(QUAS:BoTxBLC-GFP)* did not actively avoid the end of the tank where cadaverine was introduced (Supplementary figure 4) as did their sibling controls.

The *Tg(lratd2a:QF2)* driver line is expected to inhibit *lratd2a*-expressing neurons in both the vHb as well as in the right dHb. We therefore devised an intersectional strategy that combines Cre/lox mediated recombination (Förster et al., 2017; Satou et al., 2013; Tabor et al., 2019) and the QF2/QUAS system (Ghosh and Halpern, 2016; Subedi *et al.*, 2014) to block the activity of neurons selectively in the right dHb. We produced transgenic fish expressing Cre recombinase under the control of the endogenous *solute carrier family 5 member 7a* (*slc5a7a*) gene using CRISPR/Cas9 targeted integration (Kimura *et al.*, 2014) (Figures 3A-B). *slc5a7a* encodes a choline transporter involved in acetylcholine biosynthesis and, in zebrafish larvae, is strongly expressed in the right dHb and not in the vHb (Hong *et al.*, 2013). Accordingly, in larvae bearing the three transgenes *Tg(lratd2a:QF2)*^{c601}, *Tg(slc5a7a:Cre)*^{c662} and *Tg(QUAS:loxP-mCherry-loxP-GFP-CAAX)*^{c679} Cre-mediated recombination resulted in a switch in reporter labeling from red to green in right dHb neurons (Figure 3C). We followed a similar approach to inhibit synaptic transmission from *lratd2a* right dHb neurons using Botulinum neurotoxin (Lal *et al.*, 2018;

309 Sternberg *et al.*, 2016; Zhang *et al.*, 2017). A *BoTxBLC-GFP* fusion protein was placed
310 downstream of a floxed *mCherry* reporter to make *Tg(QUAS:loxP-mCherry-loxP-BoTxBLC-*
311 *GFP)*^{c674}. To validate the effectiveness of this transgenic line, a neuron specific promoter from a
312 Xenopus neural-specific beta tubulin (*Xla.Tubb2*) gene (Peri and Nusslein-Volhard, 2008) was
313 used to drive QF2 expression. Larvae bearing *Tg(Xla.Tubb2:QF2;he1.1:mCherry)*^{c663};
314 *Tg(slc5a7a:Cre)*^{c662} and *Tg(QUAS:loxP-mCherry-loxP-BoTxBLC-GFP)*^{c674} showed a
315 significantly reduced response to a touch stimulus, indicating that the neurotoxin was produced in
316 the presence of Cre recombinase (Supplementary figure 5, Supplementary movie 1).

317 *BoTxBLC-GFP* was selectively expressed in *lratd2a*/*slc5a7a* neurons of the right dHb
318 (Figure 3D and Supplementary figure 6) in larvae bearing the three transgenes
319 *Tg(lratd2a:QF2)*^{c601}*, Tg(slc5a7a:Cre)*^{c662} and *Tg(QUAS:loxP-mCherry-loxP-BoTxBLC-GFP)*^{c674}.
320 Axons labeled by *BoTxBLC-GFP* terminated at the vIPN in the same location as those observed
321 in *Tg(lratd2a:QF2)* (Figure 3E), suggesting that botulinum neurotoxin inhibits synaptic
322 transmission within this restricted region of the vIPN.

323 To determine whether the *lratd2a* neurons in the right dHb contributed to the aversive
324 response to cadaverine, we monitored behavior following its addition . During the first two minutes
325 following exposure, adults both expressing or not expressing *BoTxBLC-GFP* avoided cadaverine.
326 However, the aversive response was sustained for 4 min in control fish, but not in those expressing
327 *BoTxBLC-GFP* in the *lratd2a* neurons of the right dHb (Figures 3F-G). These findings indicate
328 that this subset of right dHb neurons are required for a prolonged aversive response to cadaverine.

329 Disruption of synaptic transmission in *lratd2a*-expressing Hb neurons alone did not alter
330 the response of zebrafish to alarm substance, which typically triggers erratic, rapid swimming and
331 bottom dwelling, followed by freezing behavior (Diaz-Verdugo et al., 2019; Jesuthasan and

Mathuru, 2008). Similar to controls, both juveniles and adults expressing *BoTxBLC-GFP* under the control of *Tg(lratd2a:QF2)*^{c601} showed rapid swimming/darting behavior within 22-25 second after delivery of alarm substance, first doubling their speed of swimming (Figures 3H-J and Supplementary figure 7), and then freezing for the duration of the 5 min recording period Blocking the activity of *lratd2a* neurons in the right dHb and in the bilateral vHb is therefore insufficient to diminish the robust behavioral changes elicited by alarm substance (Figures 3H-J and Supplementary figures 4C-D).

Zebrafish mutants with habenular defects show altered responses to aversive cues

We examined the response to aversive odorants by *tcf7l2*^{zf55} mutants that develop with symmetric left-isomerized dHb and lack the vHb, but are viable to adulthood (Husken et al., 2014). In agreement with the transformation of dHb identity, projections from OB mitral cells do not terminate in the right dHb of homozygous mutants nor are *lratd2a*-expressing neurons or their efferents to the vIPN detected (Figures 4A-D).

Following application of cadaverine, *tcf7l2*^{zf55} homozygous adults did not exhibit the characteristic avoidance behavior of their wild type siblings (Figure 4E). Exposure to alarm substance also did not elicit a significant increase in their swimming speed from baseline (1.13 ± 0.22 cm/sec before and 1.89 ± 0.56 cm/sec after) relative to WT siblings (2.84 ± 0.48 cm/sec before and 4.88 ± 0.63 cm/sec after, Figure 4F). However, homozygous *tcf7l2*^{zf5} mutants tended to spend more time swimming in the top half of a novel test tank than wild-type adults, a behavior that was suppressed in the presence of alarm substance (Fig. 4G).

To further assess the role of *lratd2a*-expressing neurons in aversive olfactory processing, we looked at homozygous mutants of the *brain-specific homeobox* (*bsx*) gene, which develop

355 right-isomerized dHb [(Schredelseker and Driever, 2018) and Figure 5A] and are viable to
356 adulthood (Schredelseker and Driever, 2018). As might be expected when both dHb have right
357 identity, equivalent populations of *lratd2a*-expressing neurons were found on both sides of the
358 brain (Figure 5C). Instead of innervating only the right dHb as in controls, the axons of *lhx2a*:*gap-*
359 *YFP* labeled olfactory mitral cells terminated in the left and right dHb [(Dreosti *et al.*, 2014) and
360 Figure 5B], where the clusters of *lratd2a* neurons are situated (data not shown). Projections from
361 the *lratd2a* dHb neurons coursed bilaterally through the left and right fasciculus retroflexus (FR)
362 and innervated the same limited region of the ventral IPN (Figure 5C).

363 To measure the reaction to cadaverine in bsx^{m1376} homozygous adults with bilaterally
364 symmetric *lratd2a* neurons, we counted the number of cells expressing *fos* in the dHb and found
365 an increase in the left nucleus compared to heterozygous siblings (Figure 5E, Supplementary figure
366 8). Despite the symmetric activation of dHb neurons, $bsx^{m1376/m1376}$ mutants did not exhibit
367 increased avoidance to cadaverine compared to controls (Figure 5D). Overall, homozygous
368 mutants were slower swimmers than heterozygotes; however, after exposure to alarm substance,
369 their swimming speed relative to baseline was two-fold faster than that of their heterozygous
370 siblings (Figure 5F), indicative of an enhanced response to this aversive cue.
371

Discussion

From worms to humans, stimuli including odors are differently perceived by left and right sensory organs to elicit distinct responses (Gunturkun and Ocklenburg, 2017; Güntürkün et al., 2020). Honeybees, for example, show an enhanced performance in olfactory learning when their right antenna is trained to odors (Guo et al., 2016; Letzkus et al., 2006; Rogers and Vallortigara, 2008). In mice, over one third of mitral/tufted cells were found to be interconnected between the ipsilateral and contralateral olfactory bulbs for sharing of odor information received separately from each nostril, and for coordinated perception (Grobman et al., 2018). The zebrafish provides a notable example of a lateralized olfactory pathway, with the discovery of a subset of bilateral mitral cells that project to the dorsal habenulae but terminate only at the right nucleus (Miyasaka *et al.*, 2014; Miyasaka *et al.*, 2009). This finding prompted us to ask what is different about the post-synaptic dHb neurons that receive this olfactory input and what function does this asymmetric pathway serve.

Aversive olfactory cues activate identified neurons in the right dHb

We previously showed that the olfactory mitral cells that express *lhx2a* and are located in medio-dorsal and ventro-medial bilateral glomerular clusters (Miyasaka *et al.*, 2014; Miyasaka *et al.*, 2009) project their axons to a subregion of the right dHb where the *lratd2a* gene is transcribed (deCarvalho *et al.*, 2013). From transgenic labeling with membrane-tagged fluorescent proteins, we now confirm that the *lhx2a* olfactory neurons precisely terminate at a cluster of *lratd2a*/*slc5a7a* expressing cholinergic neurons present in the right but not the left dHb.

From calcium imaging, we validated that the right dHb appears more responsive than the left when larval zebrafish are exposed to aversive odors such as cadaverine or chondroitin sulfate

(Jetti *et al.*, 2014; Krishnan *et al.*, 2014), a component of alarm substance (Mathuru *et al.*, 2012), and further determined that the *lratd2a*-expressing neurons of the right dHb specifically respond to these aversive olfactory cues. As has also been observed by others (Jesuthasan et al., 2020), application of vehicle alone, even when introduced slowly into a testing chamber, is sufficient to elicit a change in GCaMP fluorescence. Determining the habenular response to odorants relative to vehicle alone is thus an essential measure, but one that has not been reported in all studies (Chen *et al.*, 2019; Jetti *et al.*, 2014; Krishnan *et al.*, 2014).

In adults, we used *fos* expression as a measure of neuronal activation and showed that transcripts colocalized to *lratd2a*-expressing cells. Interestingly, cadaverine predominantly activated neurons in the right dHb in larvae and adults, whereas neurons responsive to alarm substance were detected in both the left and right dHb nuclei of adult zebrafish. Different types of olfactory cues activate distinct glomeruli in the OB (Friedrich and Korsching, 1997; Yoshihara, 2014), and consistent with the prior studies, we observed that, in adults, cadaverine significantly increased *fos* expression in the mdG and dG regions, the location of *lhx2a* neurons that project to the right dHb. By contrast, alarm substance predominantly activated neurons in the lG and dlG regions of the OB that innervate the telencephalon and posterior tuberculum (Miyasaka *et al.*, 2014; Miyasaka *et al.*, 2009), suggesting that both dHb receive input via this route rather than through direct olfactory connections. Indeed, we found that more neurons reacted to alarm substance than cadaverine throughout the brain, including in the Dp, Vv and thalamic areas (data not shown).

In previous experiments (deCarvalho *et al.*, 2013), we did not detect activated neurons in the right dHb of adult zebrafish following exposure to cadaverine or alarm substance. Several factors could account for the difference from the earlier study: we now have the transgenic tools

418 to examine *lratd2a* neurons directly, we used higher concentrations of cadaverine and alarm
419 substance and, in contrast to delivering odorants to groups of zebrafish, we tested the neuronal
420 response in individual adults.

421 It has been suggested that lateralized olfactory and visual functions of the dHb are more
422 prominent early in development and less so at later stages (Fore et al., 2020). However, the
423 presence of *lratd2a*-expressing neurons in the right dHb and their preferential response to
424 cadaverine from larval to juvenile and adult stages supports the persistence of lateralized activity
425 and illustrates the value of examining defined neuronal populations.

426

427 **Right dHb neurons mediate aversive behavioral responses**

428 Despite both being aversive cues (Hussain *et al.*, 2013; Mathuru *et al.*, 2012), cadaverine
429 and alarm substance elicit different behavioral responses by adult zebrafish. Control fish show
430 active avoidance to cadaverine for the first to 2 to 4 minutes of a 5 minute testing period, whereas
431 alarm substance triggers immediate erratic behavior such as rapid swimming and darting that is
432 typically followed by prolonged freezing (Hussain *et al.*, 2013; Mathuru *et al.*, 2012).

433 We found that perturbation of the *lratd2a*-expressing right dHb neurons either selectively
434 by *BoTxBLC*-mediated synaptic inactivation, or in *tcf7l2*^{zf55} homozygous mutants that completely
435 lack them, reduced avoidance to cadaverine, either in the length or degree of the response.

436 However, juveniles or adults with *BoTxBLC* inactivated neurons displayed a similar
437 response to alarm substance as controls. In contrast, *tcf7l2*^{zf55} mutants, showed no difference in
438 their swimming behavior before and after its addition. One explanation is that many regions
439 throughout the brain are likely involved in directing the complex repertoire of behaviors elicited
440 by alarm substance and inactivation of *lratd2a* neurons in the habenular region alone is insufficient

441 to weaken the overall response. Our findings also rule out a role for the ventral habenulae in the
442 response to alarm substance, as the reaction to alarm substance was intact in transgenic adults in
443 which *lratd2a* neurons were inactivated by *BoTxBLC* in the bilateral vHb as well as in the right
444 dHb. Alternatively, the *tcf7l2*^{zf55} mutation could disrupt other brain regions that regulate behaviors
445 elicited by alarm substance since the *tfc7l2* gene is expressed in neurons throughout the brain,
446 including the anterior tectum, dorsal thalamus and the hindbrain (Young et al., 2002).

447 Similar to *tcf7l2*^{zf5}, the *bsx*^{m1376} mutation is pleiotropic not only resulting in right-
448 isomerization of the dHb due to the absence of the parapineal (Schredelseker and Driever, 2018),
449 but also loss of the terminal tuberal hypothalamus, mammillary hypothalamic regions and
450 secondary prosencephalon (Schredelseker et al., 2020). Although homozygous mutants showed a
451 hyperactive response to alarm substance relative to controls, we cannot discount the involvement
452 of other affected brain regions. Albeit technically challenging in adults, a more selective test such
453 as optogenetic activation of only the *lratd2a* dHb neurons in wild-type and mutant zebrafish could
454 help resolve their contribution to the alarm response.

455 The identification of a subset of neurons in the right dHb that receive olfactory input and
456 terminate their axons at a defined subregion of the ventral IPN lays the groundwork for tracing an
457 entire pathway from olfactory receptors to the neurons directing the appropriate behavioral
458 response. The midline IPN has been morphologically defined into subregions (deCarvalho *et al.*,
459 2014; Lima et al., 2017; Quina et al., 2017), but their connectivity and functional properties have
460 been understudied. Recent work has begun to assign different functions to given subregions, such
461 as the role of the rostral IPN in nicotine aversion (Morton et al., 2018; Quina *et al.*, 2017). Neurons
462 in the ventral IPN project to the raphe nucleus (Agetsuma et al., 2010; Lima *et al.*, 2017), but the
463 precise identity of raphe neurons that are innervated by the *lratd2a*-expressing dHb neurons

464 remains to be determined. Transcriptional profiling of the IPN should yield useful information on
465 its diverse neuronal populations and likely lead to the identification of the relevant post-synaptic
466 targets in the ventral IPN and their efferent connections. Elaboration of this pathway may also help
467 explain the advantage of lateralization in the processing of aversive information. It has been
468 argued, for instance, that the antennal specialization to aversive odors in bees is correlated with
469 directed turning away from the stimulus and escape (Rogers and Vallortigara, 2019). Beyond
470 olfaction, left-right asymmetry appears to be a more general feature of stress-inducing, aversive
471 responses as demonstrated for the rat ventral hippocampus (Sakaguchi and Sakurai, 2017) and
472 human pre-frontal cortex, where heightened anxiety also activates more neurons on the right than
473 on the left (Avram et al., 2010; Ocklenburg et al., 2016).
474
475

References

Agetsuma, M., Aizawa, H., Aoki, T., Nakayama, R., Takahoko, M., Goto, M., Sassa, T., Amo, R., Shiraki, T., Kawakami, K., et al. (2010). The habenula is crucial for experience-dependent modification of fear responses in zebrafish. Nat Neurosci *13*, 1354-1356. 10.1038/nn.2654.

Amo, R., Aizawa, H., Takahoko, M., Kobayashi, M., Takahashi, R., Aoki, T., and Okamoto, H. (2010). Identification of the Zebrafish Ventral Habenula As a Homolog of the Mammalian Lateral Habenula. The Journal of Neuroscience *30*, 1566-1574. 10.1523/jneurosci.3690-09.2010.

Auer, T.O., Duroure, K., De Cian, A., Concordet, J.-P., and Del Bene, F. (2014). Highly efficient CRISPR/Cas9-mediated knock-in in zebrafish by homology-independent DNA repair. Genome research *24*, 142-153. 10.1101/gr.161638.113.

Avram, J., Balteş, F.R., Miclea, M., and Miu, A.C. (2010). Frontal EEG Activation Asymmetry Reflects Cognitive Biases in Anxiety: Evidence from an Emotional Face Stroop Task. Applied Psychophysiology and Biofeedback *35*, 285-292. 10.1007/s10484-010-9138-6.

Chen, W.-y., Peng, X.-l., Deng, Q.-s., Chen, M.-j., Du, J.-l., and Zhang, B.-b. (2019). Role of Olfactorily Responsive Neurons in the Right Dorsal Habenula–Ventral Interpeduncular Nucleus Pathway in Food-Seeking Behaviors of Larval Zebrafish. Neuroscience *404*, 259-267. https://doi.org/10.1016/j.neuroscience.2019.01.057.

deCarvalho, T.N., Akitake, C.M., Thisse, C., Thisse, B., and Halpern, M.E. (2013). Aversive cues fail to activate fos expression in the asymmetric olfactory-habenula pathway of zebrafish. Front Neural Circuits *7*, 98. 10.3389/fncir.2013.00098.

deCarvalho, T.N., Subedi, A., Rock, J., Harfe, B.D., Thisse, C., Thisse, B., Halpern, M.E., and Hong, E. (2014). Neurotransmitter map of the asymmetric dorsal habenular nuclei of zebrafish. genesis *52*, 636-655. 10.1002/dvg.22785.

Diaz-Verdugo, C., Sun, G.J., Fawcett, C.H., Zhu, P., and Fishman, M.C. (2019). Mating Suppresses Alarm Response in Zebrafish. Current Biology *29*, 2541-2546.e2543. 10.1016/j.cub.2019.06.047.

Dieris, M., Ahuja, G., Krishna, V., and Korsching, S.I. (2017). A single identified glomerulus in the zebrafish olfactory bulb carries the high-affinity response to death-associated odor cadaverine. Scientific reports *7*, 40892. 10.1038/srep40892.

Dreosti, E., Vendrell Llopis, N., Carl, M., Yaksi, E., and Wilson, S.W. (2014). Left-right asymmetry is required for the habenulae to respond to both visual and olfactory stimuli. Curr Biol *24*, 440-445. 10.1016/j.cub.2014.01.016.

508 Duboué, E.R., Hong, E., Eldred, K.C., and Halpern, M.E. (2017). Left Habenular Activity
509 Attenuates Fear Responses in Larval Zebrafish. Current Biology *27*, 2154-2162 e2153.
510 https://doi.org/10.1016/j.cub.2017.06.017.

511 Facchin, L., Duboué, E.R., and Halpern, M.E. (2015). Disruption of Epithalamic Left–Right
512 Asymmetry Increases Anxiety in Zebrafish. The Journal of Neuroscience *35*, 15847-15859.
513 10.1523/jneurosci.2593-15.2015.

514 Fore, S., Acuña-Hinrichsen, F., Mutlu, K.A., Bartoszek, E.M., Serneels, B., Faturos, N.G., Chau,
515 K.T.P., Cosacak, M.I., Verdugo, C.D., Palumbo, F., et al. (2020). Functional properties of
516 habenular neurons are determined by developmental stage and sequential neurogenesis. Science
517 Advances *6*, eaaz3173. 10.1126/sciadv.aaz3173.

518 Friedrich, R.W., and Korsching, S.I. (1997). Combinatorial and Chemotopic Odorant Coding in
519 the Zebrafish Olfactory Bulb Visualized by Optical Imaging. Neuron *18*, 737-752. 10.1016/S0896-
520 6273(00)80314-1.

521 Förster, D., Arnold-Ammer, I., Laurell, E., Barker, A.J., Fernandes, A.M., Finger-Baier, K., Filosa,
522 A., Helmbrecht, T.O., Kölsch, Y., Kühn, E., et al. (2017). Genetic targeting and anatomical
523 registration of neuronal populations in the zebrafish brain with a new set of BAC transgenic tools.
524 Scientific reports *7*, 5230. 10.1038/s41598-017-04657-x.

525 Gamse, J.T., Shen, Y.C., Thisse, C., Thisse, B., Raymond, P.A., Halpern, M.E., and Liang, J.O.
526 (2002). Otx5 regulates genes that show circadian expression in the zebrafish pineal complex. Nat
527 Genet *30*, 117-121. 10.1038/ng793.

528 Ghosh, A., and Halpern, M.E. (2016). Chapter 10 - Transcriptional regulation using the Q system
529 in transgenic zebrafish. In Methods in cell biology, M.W. H. William Detrich, and I.Z. Leonard,
530 eds. (Academic Press), pp. 205-218. http://dx.doi.org/10.1016/bs.mcb.2016.05.001.

531 Grobman, M., Dalal, T., Lavian, H., Shmuel, R., Belelovsky, K., Xu, F., Korngreen, A., and
532 Haddad, R. (2018). A Mirror-Symmetric Excitatory Link Coordinates Odor Maps across Olfactory
533 Bulbs and Enables Odor Perceptual Unity. Neuron *99*, 800-813.e806.
534 https://doi.org/10.1016/j.neuron.2018.07.012.

535 Gunturkun, O., and Ocklenburg, S. (2017). Ontogenesis of Lateralization. Neuron *94*, 249-263.
536 10.1016/j.neuron.2017.02.045.

537 Guo, Y., Wang, Z., Li, Y., Wei, G., Yuan, J., Sun, Y., Wang, H., Qin, Q., Zeng, Z., Zhang, S., and
538 Chen, R. (2016). Lateralization of gene expression in the honeybee brain during olfactory learning.
539 Scientific reports *6*, 34727-34727. 10.1038/srep34727.

Güntürkün, O., Ströckens, F., and Ocklenburg, S. (2020). Brain Lateralization: A Comparative Perspective. Physiological Reviews *100*, 1019-1063. 10.1152/physrev.00006.2019.

Hikosaka, O. (2010). The habenula: from stress evasion to value-based decision-making. Nat Rev Neurosci *11*, 503-513. 10.1038/nrn2866.

Hong, E., Santhakumar, K., Akitake, C.A., Ahn, S.J., Thisse, C., Thisse, B., Wyart, C., Mangin, J.-M., and Halpern, M.E. (2013). Cholinergic left-right asymmetry in the habenulo-interpeduncular pathway. Proceedings of the National Academy of Sciences *110*, 21171-21176. 10.1073/pnas.1319566110.

Hsu, Y.-W.A., Morton, G., Guy, E.G., Wang, S.D., and Turner, E.E. (2016). Dorsal Medial Habenula Regulation of Mood-Related Behaviors and Primary Reinforcement by Tachykinin-Expressing Habenula Neurons. eneuro *3*. 10.1523/eneuro.0109-16.2016.

Husken, U., Stickney, H.L., Gestri, G., Bianco, I.H., Faro, A., Young, R.M., Roussigne, M., Hawkins, T.A., Beretta, C.A., Brinkmann, I., et al. (2014). Tcf7l2 is required for left-right asymmetric differentiation of habenular neurons. Curr Biol *24*, 2217-2227. 10.1016/j.cub.2014.08.006.

Hussain, A., Saraiva, L.R., Ferrero, D.M., Ahuja, G., Krishna, V.S., Liberles, S.D., and Korsching, S.I. (2013). High-affinity olfactory receptor for the death-associated odor cadaverine. Proceedings of the National Academy of Sciences *110*, 19579-19584. 10.1073/pnas.1318596110.

Hwang, W.Y., Fu, Y., Reyon, D., Maeder, M.L., Tsai, S.Q., Sander, J.D., Peterson, R.T., Yeh, J.R., and Joung, J.K. (2013). Efficient genome editing in zebrafish using a CRISPR-Cas system. Nat Biotechnol *31*, 227-229. 10.1038/nbt.2501.

Jao, L.E., Wente, S.R., and Chen, W. (2013). Efficient multiplex biallelic zebrafish genome editing using a CRISPR nuclease system. Proceedings of the National Academy of Sciences of the United States of America *110*, 13904-13909. 10.1073/pnas.1308335110.

Jesuthasan, S., Krishnan, S., Cheng, R.-K., and Mathuru, A. (2020). Neural correlates of state transitions elicited by a chemosensory danger cue. Progress in Neuro-Psychopharmacology and Biological Psychiatry, 110110. https://doi.org/10.1016/j.pnpbp.2020.110110.

Jesuthasan, S.J., and Mathuru, A.S. (2008). The alarm response in zebrafish: innate fear in a vertebrate genetic model. J Neurogenet *22*, 211-228. 10.1080/01677060802298475.

Jetti, S.K., Vendrell-Llopis, N., and Yaksi, E. (2014). Spontaneous activity governs olfactory representations in spatially organized habenular microcircuits. Curr Biol *24*, 434-439. 10.1016/j.cub.2014.01.015.

572 Kimura, Y., Hisano, Y., Kawahara, A., and Higashijima, S. (2014). Efficient generation of knock-
573 in transgenic zebrafish carrying reporter/driver genes by CRISPR/Cas9-mediated genome
574 engineering. Sci Rep *4*, 6545. 10.1038/srep06545.

575 Koide, T., Miyasaka, N., Morimoto, K., Asakawa, K., Urasaki, A., Kawakami, K., and Yoshihara,
576 Y. (2009). Olfactory neural circuitry for attraction to amino acids revealed by transposon-mediated
577 gene trap approach in zebrafish. Proceedings of the National Academy of Sciences *106*, 9884-
578 9889. 10.1073/pnas.0900470106.

579 Krishnan, S., Mathuru, A.S., Kibat, C., Rahman, M., Lupton, C.E., Stewart, J., Claridge-Chang,
580 A., Yen, S.C., and Jesuthasan, S. (2014). The right dorsal habenula limits attraction to an odor in
581 zebrafish. Curr Biol *24*, 1167-1175. 10.1016/j.cub.2014.03.073.

582 Kwan, K.M., Fujimoto, E., Grabher, C., Mangum, B.D., Hardy, M.E., Campbell, D.S., Parant,
583 J.M., Yost, H.J., Kanki, J.P., and Chien, C.-B. (2007). The Tol2kit: A multisite gateway-based
584 construction kit for Tol2 transposon transgenesis constructs. Developmental Dynamics *236*, 3088-
585 3099. 10.1002/dvdy.21343.

586 Lal, P., Tanabe, H., Suster, M.L., Ailani, D., Kotani, Y., Muto, A., Itoh, M., Iwasaki, M., Wada,
587 H., Yaksi, E., and Kawakami, K. (2018). Identification of a neuronal population in the
588 telencephalon essential for fear conditioning in zebrafish. BMC Biology *16*, 45. 10.1186/s12915-
589 018-0502-y.

590 Letzkus, P., Ribi, W.A., Wood, J.T., Zhu, H., Zhang, S.-W., and Srinivasan, M.V. (2006).
591 Lateralization of Olfaction in the Honeybee Apis mellifera. Current Biology *16*, 1471-1476.
592 10.1016/j.cub.2006.05.060.

593 Lima, L.B., Bueno, D., Leite, F., Souza, S., Gonçalves, L., Furigo, I.C., Donato, J., and Metzger,
594 M. (2017). Afferent and efferent connections of the interpeduncular nucleus with special reference
595 to circuits involving the habenula and raphe nuclei. Journal of Comparative Neurology *525*, 2411-
596 2442. 10.1002/cne.24217.

597 Mathuru, Ajay S., Kibat, C., Cheong, Wei F., Shui, G., Wenk, Markus R., Friedrich, Rainer W.,
598 and Jesuthasan, S. (2012). Chondroitin Fragments Are Odorants that Trigger Fear Behavior in
599 Fish. Current Biology *22*, 538-544. http://dx.doi.org/10.1016/j.cub.2012.01.061.

600 Miyasaka, N., Arganda-Carreras, I., Wakisaka, N., Masuda, M., Sumbul, U., Seung, H.S., and
601 Yoshihara, Y. (2014). Olfactory projectome in the zebrafish forebrain revealed by genetic single-
602 neuron labelling. Nature communications *5*, 3639. 10.1038/ncomms4639.

603 Miyasaka, N., Morimoto, K., Tsubokawa, T., Higashijima, S., Okamoto, H., and Yoshihara, Y.
604 (2009). From the olfactory bulb to higher brain centers: genetic visualization of secondary
605 olfactory pathways in zebrafish. The Journal of neuroscience *29*, 4756-4767.
606 10.1523/JNEUROSCI.0118-09.2009.

607 Morton, G., Nasirova, N., Sparks, D.W., Brodsky, M., Sivakumaran, S., Lambe, E.K., and Turner,
608 E.E. (2018). Chrna5-Expressing Neurons in the Interpeduncular Nucleus Mediate Aversion
609 Primed by Prior Stimulation or Nicotine Exposure. The Journal of Neuroscience *38*, 6900-6920.
610 10.1523/jneurosci.0023-18.2018.

611 Muncan, V., Faro, A., Haramis, A.-P.G., Hurlstone, A.F.L., Wienholds, E., van Es, J., Korving, J.,
612 Begthel, H., Zivkovic, D., and Clevers, H. (2007). T-cell factor 4 (Tcf7l2) maintains proliferative
613 compartments in zebrafish intestine. EMBO reports *8*, 966-973. 10.1038/sj.embor.7401071.

614 Ocklenburg, S., Korte, S.M., Peterburs, J., Wolf, O.T., and Güntürkün, O. (2016). Stress and
615 laterality – The comparative perspective. Physiology & Behavior *164*, 321-329.
616 https://doi.org/10.1016/j.physbeh.2016.06.020.

617 Okamoto, H., Agetsuma, M., and Aizawa, H. (2012). Genetic dissection of the zebrafish habenula,
618 a possible switching board for selection of behavioral strategy to cope with fear and anxiety.
619 Developmental neurobiology *72*, 386-394. 10.1002/dneu.20913.

620 Peri, F., and Nusslein-Volhard, C. (2008). Live imaging of neuronal degradation by microglia
621 reveals a role for v0-ATPase a1 in phagosomal fusion in vivo. Cell *133*, 916-927.
622 10.1016/j.cell.2008.04.037.

623 Potter, C.J., Tasic, B., Russler, E.V., Liang, L., and Luo, L. (2010). The Q System: A Repressible
624 Binary System for Transgene Expression, Lineage Tracing, and Mosaic Analysis. Cell *141*, 536-
625 548. 10.1016/j.cell.2010.02.025.

626 Quina, L.A., Harris, J., Zeng, H., and Turner, E.E. (2017). Specific connections of the
627 interpeduncular subnuclei reveal distinct components of the habenulopeduncular pathway. Journal
628 of Comparative Neurology *525*, n/a-n/a. 10.1002/cne.24221.

629 Rogers, L.J., and Vallortigara, G. (2008). From antenna to antenna: lateral shift of olfactory
630 memory recall by honeybees. PloS one *3*, e2340-e2340. 10.1371/journal.pone.0002340.

631 Rogers, L.J., and Vallortigara, G. (2019). Complementary Specializations of the Left and Right
632 Sides of the Honeybee Brain. Front Psychol *10*, 280. 10.3389/fpsyg.2019.00280.

633 Sakaguchi, Y., and Sakurai, Y. (2017). Left–right functional asymmetry of ventral hippocampus
634 depends on aversiveness of situations. Behavioural Brain Research *325*, 25-33.
635 https://doi.org/10.1016/j.bbr.2017.02.028.

636 Sander, J.D., Maeder, M.L., Reyon, D., Voytas, D.F., Joung, J.K., and Dobbs, D. (2010). ZiFiT
637 (Zinc Finger Targeter): an updated zinc finger engineering tool. Nucleic Acids Research *38*,
638 W462-W468. 10.1093/nar/gkq319.

639 Satou, C., Kimura, Y., Hirata, H., Suster, M.L., Kawakami, K., and Higashijima, S.-i. (2013).
640 Transgenic tools to characterize neuronal properties of discrete populations of zebrafish neurons.
641 Development *140*, 3927-3931. 10.1242/dev.099531.

642 Schindelin, J., Arganda-Carreras, I., Frise, E., Kaynig, V., Longair, M., Pietzsch, T., Preibisch, S.,
643 Rueden, C., Saalfeld, S., Schmid, B., et al. (2012). Fiji: an open-source platform for biological-
644 image analysis. Nature methods *9*, 676. 10.1038/nmeth.2019
645 https://www.nature.com/articles/nmeth.2019#supplementary-information.

646 Schredelseker, T., and Driever, W. (2018). Bsx controls pineal complex development.
647 Development *145*, dev163477. 10.1242/dev.163477.

648 Schredelseker, T., Veit, F., Dorsky, R.I., and Driever, W. (2020). Bsx Is Essential for
649 Differentiation of Multiple Neuromodulatory Cell Populations in the Secondary Prosencephalon.
650 Frontiers in neuroscience *14*. 525. 10.3389/fnins.2020.00525.

651 Severi, Kristen E., Portugues, R., Marques, João C., O'Malley, Donald M., Orger, Michael B., and
652 Engert, F. (2014). Neural Control and Modulation of Swimming Speed in the Larval Zebrafish.
653 Neuron *83*, 692-707. https://doi.org/10.1016/j.neuron.2014.06.032.

654 Siniscalchi, M. (2017). Olfactory Lateralization. In Lateralized Brain Functions: Methods in
655 Human and Non-Human Species, L.J. Rogers, and G. Vallortigara, eds. (Springer New York), pp.
656 103-120. 10.1007/978-1-4939-6725-4_4.

657 Sternberg, Jenna R., Severi, Kristen E., Fidelin, K., Gomez, J., Ihara, H., Alcheikh, Y., Hubbard,
658 Jeffrey M., Kawakami, K., Suster, M., and Wyart, C. (2016). Optimization of a Neurotoxin to
659 Investigate the Contribution of Excitatory Interneurons to Speed Modulation In Vivo. Current
660 Biology *26*, 2319-2328. http://dx.doi.org/10.1016/j.cub.2016.06.037.

661 Subedi, A., Macurak, M., Gee, S.T., Monge, E., Goll, M.G., Potter, C.J., Parsons, M.J., and
662 Halpern, M.E. (2014). Adoption of the Q transcriptional regulatory system for zebrafish
663 transgenesis. Methods *66*, 433-440. 10.1016/j.ymeth.2013.06.012.

664 Suster, M.L., Abe, G., Schouw, A., and Kawakami, K. (2011). Transposon-mediated BAC
665 transgenesis in zebrafish. Nat. Protocols *6*, 1998-2021.
666 http://www.nature.com/nprot/journal/v6/n12/abs/nprot.2011.416.html#supplementary-
667 information.

668 Tabor, K.M., Marquart, G.D., Hurt, C., Smith, T.S., Geoca, A.K., Bhandiwad, A.A., Subedi, A.,
669 Sinclair, J.L., Rose, H.M., Polys, N.F., and Burgess, H.A. (2019). Brain-wide cellular resolution
670 imaging of Cre transgenic zebrafish lines for functional circuit-mapping. eLife *8*, e42687.
671 10.7554/eLife.42687.

672 Wakisaka, N., Miyasaka, N., Koide, T., Masuda, M., Hiraki-Kajiyama, T., and Yoshihara, Y.
673 (2017). An Adenosine Receptor for Olfaction in Fish. Current Biology 27. 1437-1447 e1434.
674 https://doi.org/10.1016/j.cub.2017.04.014.

675 Walker, C. (1998). Chapter 3 Haploid Screens and Gamma-Ray Mutagenesis. In Methods in Cell
676 Biology, H.W. Detrich, M. Westerfield, and L.I. Zon, eds. (Academic Press), pp. 43-70.
677 https://doi.org/10.1016/S0091-679X(08)61893-2.

678 Xie, X., Mathias, J.R., Smith, M.-A., Walker, S.L., Teng, Y., Distel, M., Köster, R.W., Sirotkin,
679 H.I., Saxena, M.T., and Mumm, J.S. (2012). Silencer-delimited transgenesis: NRSE/RE1
680 sequences promote neural-specific transgene expression in a NRSF/REST-dependent manner.
681 BMC Biology *10*, 93. 10.1186/1741-7007-10-93.

682 Yoshihara, Y. (2014). Zebrafish Olfactory System. In The Olfactory System: From Odor
683 Molecules to Motivational Behaviors, K. Mori, ed. (Springer Japan), pp. 71-96. 10.1007/978-4-
684 431-54376-3_5.

685 Young, R.M., Reyes, A.E., and Allende, M.L. (2002). Expression and splice variant analysis of
686 the zebrafish tcf4 transcription factor. Mechanisms of Development *117*, 269-273.
687 https://doi.org/10.1016/S0925-4773(02)00180-6.

688 Zhang, B.B., Yao, Y.Y., Zhang, H.F., Kawakami, K., and Du, J.L. (2017). Left Habenula Mediates
689 Light-Preference Behavior in Zebrafish via an Asymmetrical Visual Pathway. Neuron *93*, 914-
690 928. e914. 10.1016/j.neuron.2017.01.011.
691
692

Acknowledgement

We thank Shin-ichi Higashijima for the *Gbait-hsp70:Gal4* donor plasmid, Wenbiao Chen for *pT3TS nCas9n* plasmid, Koichi Kawakami for the *UAS:zBoTXBLC-GFP* construct, Paul Krieg for the *Xla.Tubb* promoter construct, Claire Wyart for *GCaMP6f* plasmid and Wolfgang Driever and Tatjana Piotrowski for providing bsx^{m1376} and $tcf7l2^{zf5}$ mutant zebrafish, respectively.

Author contributions

J-H.C. and M.E.H. conceived of and designed the study and wrote the manuscript. J-H.C. performed all of the experiments. E.D. wrote MATLAB script for analyzing behavioral experiments. M.M. constructed sgRNAs for *lratd2a* and *slc5a7a*. J-M.C. generated Tol2 constructs and transgenic lines. All authors reviewed the manuscript.

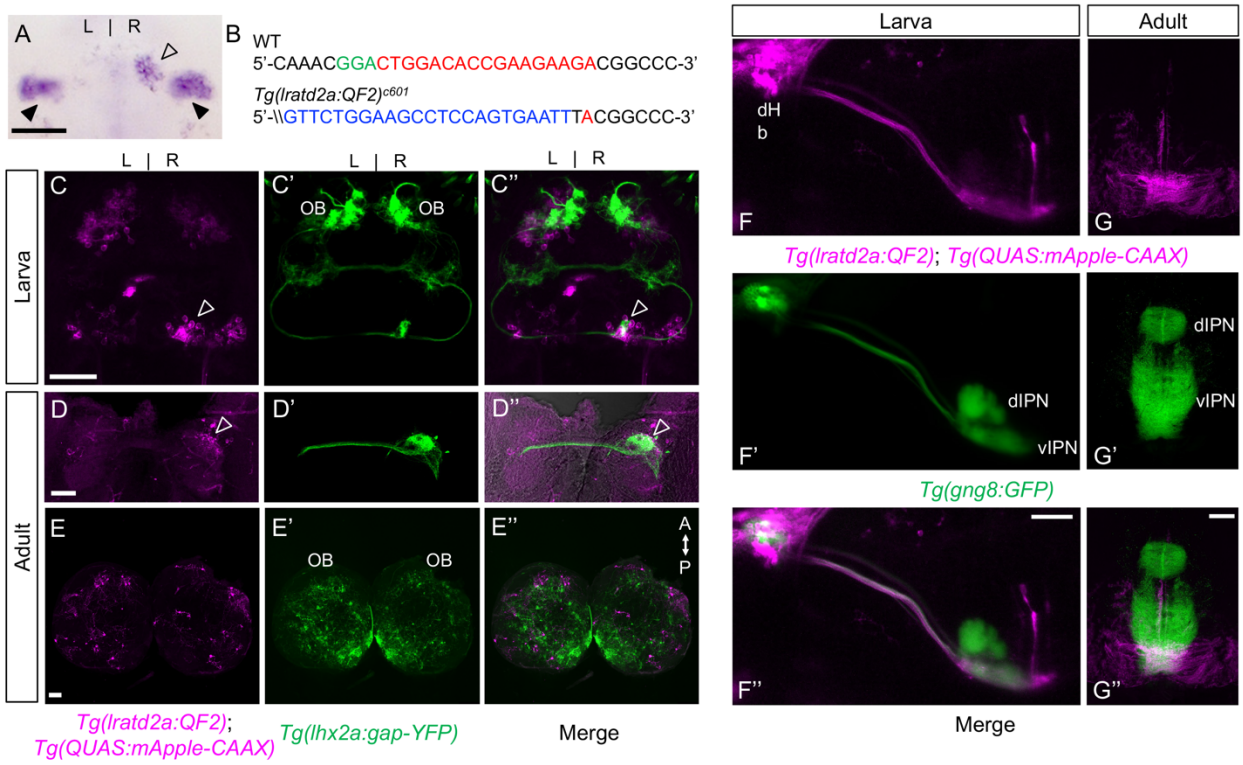

706

707 **Figure 1. *lratd2a*-expressing neurons in the right dHb connect asymmetric pathway from the**

708 **olfactory bulb to ventral IPN** (A) Pattern of *lratd2a* expression at 5 days post fertilization (dpf),

709 open arrowhead indicates right dHb and black arrowheads the bilateral vHb. (B) Sequences of WT

710 (top) and transgenic fish (bottom) with QF2 integrated within the first exon of the *lratd2a* gene.

711 PAM sequences are green, the sgRNA binding site red and donor DNA blue. Confocal dorsal

712 views of *Tg(lratd2a:QF2), Tg(QUAS:mApple-CAAX)* and *Tg(lhx2a:gap-YFP)* labeling in a (C-

713 C'') 5 dpf larva and in transverse sections of the adult brain at 3 months post-fertilization (mpf) at

714 the level of the (D-D'') dHb and (E-E'') olfactory bulb. Axons of *lhx2a* olfactory mitral cells (open

715 arrowheads, C and D) terminate at *lratd2a* dHb neurons. (F-F'') Lateral view of *Tg(lratd2a:QF2)*,

716 *Tg(QUAS:mApple-CAAX)*, *Tg(gng8:GFP)* larva at 6 dpf with mApple labeled dHb terminals at

717 the ventral interpeduncular nucleus (vIPN). Dorsal habenular nuclei (dHb), dorsal interpeduncular

718 nucleus (dIPN). (G-G'') Axonal endings of *lratd2a* dHb neurons are restricted to the ventralmost

719 region of the vIPN in transverse section of 2.5 mpf adult brain. Scale bar, 50 μm. A-P, anterior to

720 posterior; L-R, left-right; OB, olfactory bulb.

721

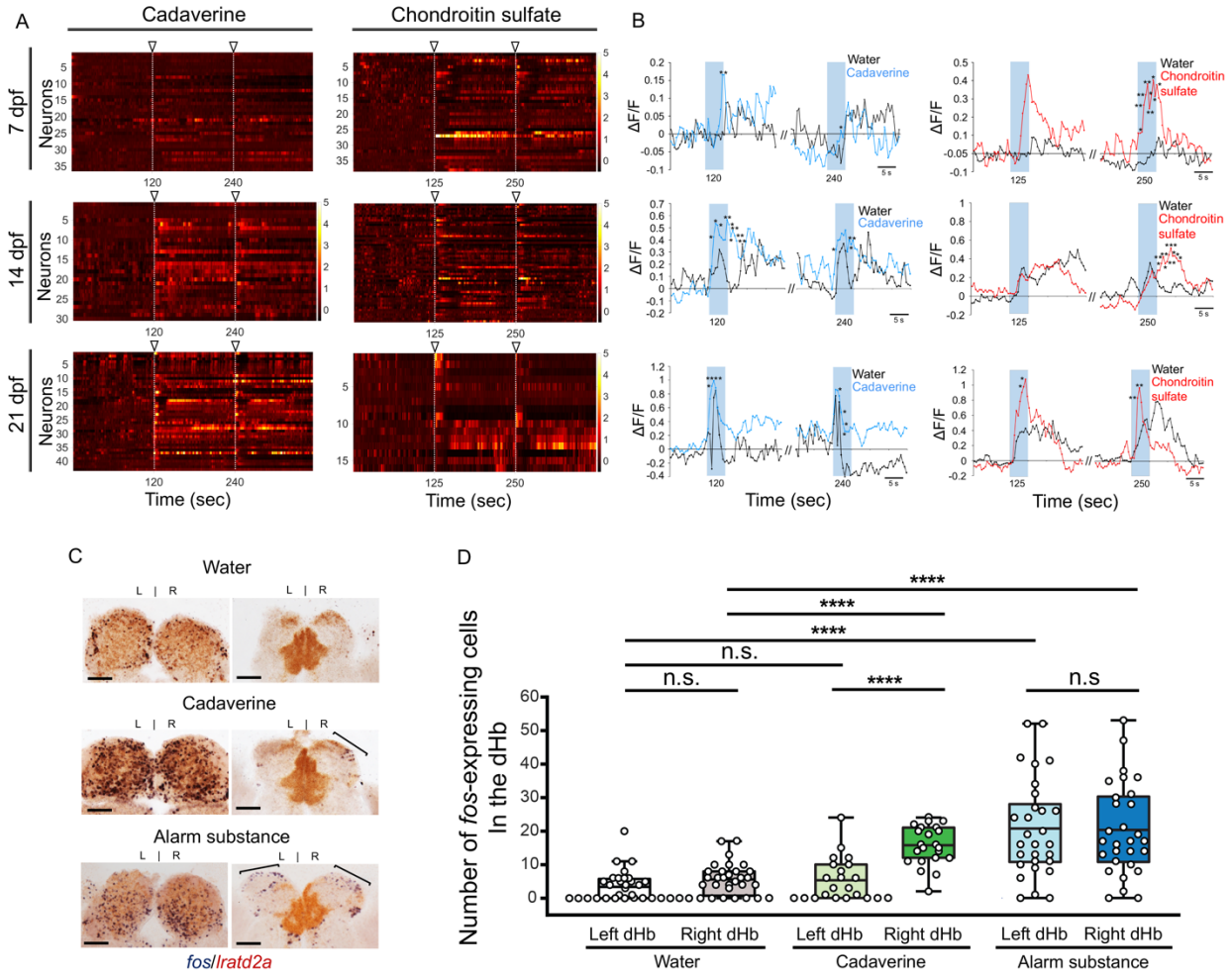

Figure 2. Increased activity of *lratd2a*-expressing dHb neurons upon exposure to aversive olfactory cues (A) Change in GCaMP fluorescence intensity (ΔF/F) of *lratd2a* neurons in the right dHb in response to cadaverine (n = 36 neurons in 5 larvae at 7 dpf, 30 neurons in 5 larvae at 14 dpf and 43 neurons in 5 larvae at 21 dpf) or chondroitin sulfate (n = 38 neurons in 4 larvae at 7 dpf, 53 neurons in 5 larvae at 14 dpf and 16 neurons in 2 larvae at 21 dpf). Open arrowheads indicate the time of odorant delivery. (B) Average change in fluorescence (ΔF/F) in seconds (sec) for all *lratd2a* positive neurons in the larval right dHb. Blue bars indicate 5 sec periods of odor delivery. (C) *fos* (blue) and *lratd2a* (brown) transcripts in adult olfactory bulbs (left panels) and

habenulae (right panels) detected by RNA *in situ* hybridization 30 min after addition of water, cadaverine or alarm substance to the test tank. Brackets indicate *fos*-expressing cells. Scale bar, 100 μm. (D) Quantification of *fos*-expressing cells in the adult dHb after addition of vehicle alone [3.58 ± 0.92 cells in the left and 5.61 ± 1.07 in the right dHb, $n = 16$ fish (Mann-Whitney $U = 349$, $P = 0.065$)], cadaverine [5.32 ± 1.36 cells in the left and 15.73 ± 1.25 in the right dHb, $n = 11$ fish (Mann-Whitney $U = 57$, P<0.00001)], or alarm substance [20.72 ± 2.70 cells in the left and 20.31 ± 2.53 in the right dHb, $n = 17$ fish (Mann-Whitney $U = 414.5$, $P = 0.928$)]. For the right dHb, significantly more cells were *fos* positive after addition of either cadaverine ($P = 5.5217E-08$) or alarm substance ($P = 3.78292E-06$). For the left dHb, a significant difference was only observed after addition of alarm substance (P=7.44458 E-07). For B and D, Student's t-test. *$P < 0.05$; **$P < 0.01$; ***$P < 0.001$; ****$P < 0.0001$; *n.s.*, not significant (P > 0.05).

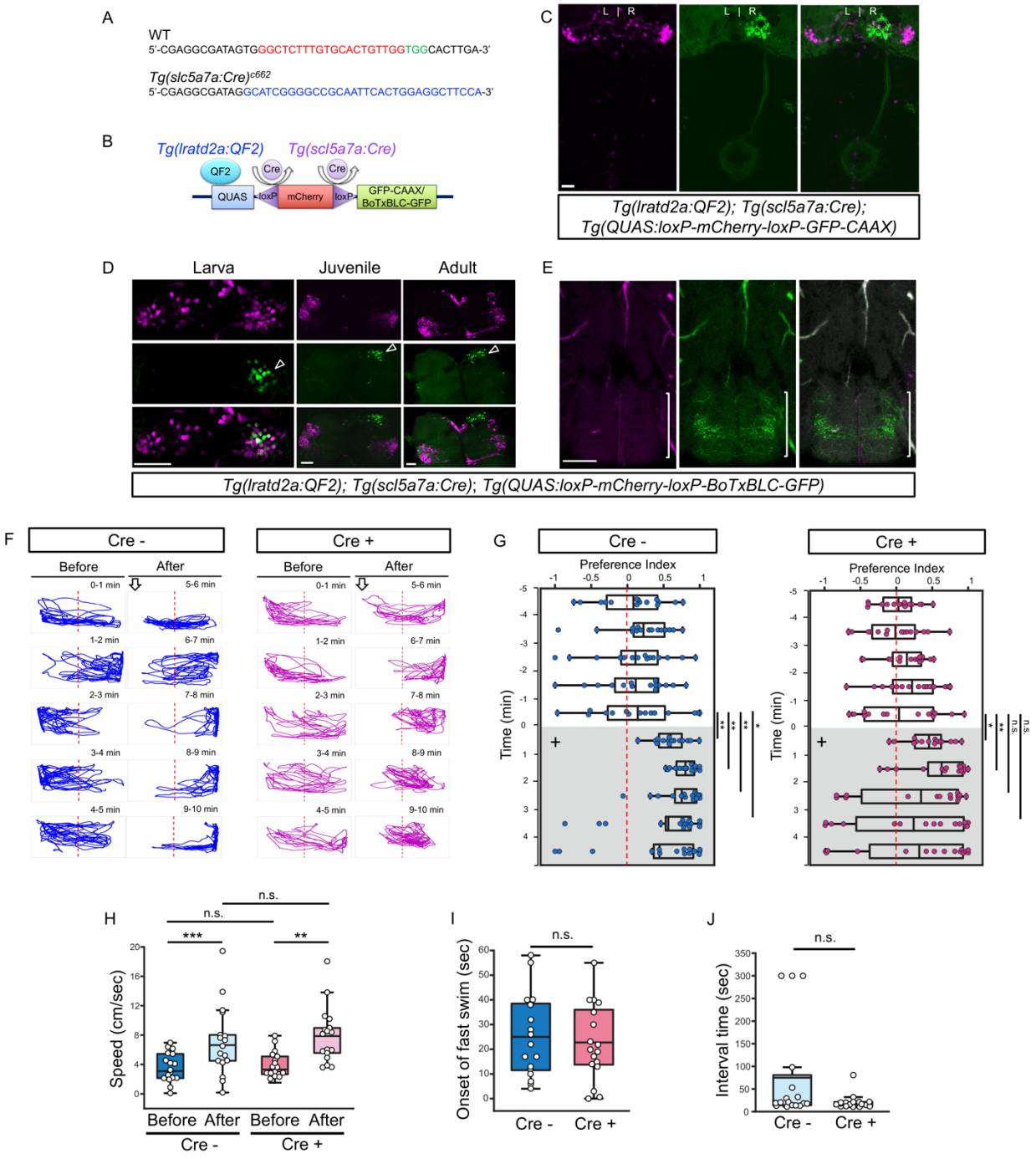

744

745 **Figure 3. Synaptic inhibition of *lratd2a* right dHb neurons attenuates response to cadaverine**

746 (A) Sequences upstream of the *slc5a7a* transcriptional start site before (WT) and after integration

747 of Cre (blue indicates donor DNA) at sgRNA target site (sgRNA binding site red and PAM

748 sequences green). (B) Schematic diagram of intersectional strategy using Cre/lox mediated

recombination and the QF2/QUAS binary system. QF2 is driven by *lratd2a* regulatory sequences and the *slc5a7a* promoter drives Cre leading to reporter/effector expression in *lratd2a* neurons in the right dHb. (C) Dorsal view of GFP labeling in only the right dHb after Cre-mediated recombination in a 5 dpf *Tg(lratd2a:QF2)*, *Tg(slc5a7a:Cre)*, *Tg(QUAS:loxP-mCherry-loxP-GFP-CAAX)* larva. Scale bar, 25 μm. (D) *BoTxBLC-GFP* labeled cells (open arrowhead) in the right dHb in *Tg(lratd2a:QF2)*, *Tg(slc5a7a:Cre)*, *Tg(QUAS:loxP-mCherry-loxP-BoTxBLC-GFP)* 5 dpf, 37 dpf and 4 mpf zebrafish. Upper images show mCherry labeled *lratd2a* Hb neurons, middle images show the subset of right dHb neurons that expressed Cre and switched to GFP, and the bottom row are merged images. Scale bar, 50 μm. (E) Transverse section of *BoTxBLC-GFP* labeled axonal endings of dHb neurons that express Cre and *lratd2a* in a subregion of the vIPN (bracket) in 37 dpf *Tg(lratd2a:QF2)*, *Tg(slc5a7a:Cre)*, *Tg(QUAS:loxP-mCherry-loxP-BoTxBLC-GFP)* juveniles. Scale bar, 50 μm. (F, G) Preferred tank location prior to and after cadaverine addition of adults genotyped for absence (Cre-, blue) or presence (Cre+, red) of *Tg(slc5a7a:Cre)*. (F) Representative 1 min traces for single Cre- and Cre+ adults recorded over 10 mins prior to (mins 0-5) and after (mins 6-10) addition of cadaverine to end of test tank (arrows). (G) Preference index for all adults tested 5 min prior to (white) and 5 min after (grey) addition of cadaverine (on + side). In Cre- fish, significant differences in avoidance behavior were detected after addition of cadaverine [6 min (P=0.0075), 7 min (P=0.0011), 8 min (P=0.0019), 9 min (P=0.032) compared to last min before addition, Student's t-test, n = 15 fish]. Cre+ fish, showed no significant differences in their preferred location beyond two mins after cadaverine addition [6 min (P=0.012), 7 min (P=0.0029) compared to last min before addition, Student's t-test, n = 15 fish]. Dashed red lines in F and G denote midpoint of test tank. (H) Swimming speed (cm/sec) during 1 min before and after addition of alarm substance for Cre- [3.61 ± 0.48 and 7.13 ± 1.15 , Student's t-test

772 (P=0.00097)], and Cre+ [4.02 ± 0.42 and 7.93 ± 0.92, Student's t-test (P=0.001)] adults. (I) Onset
773 of fast swimming after application of alarm substance was observed at 25 ± 4.05 sec in Cre- and
774 at 22.7 ± 3.72 sec in Cre+ fish. (J) Time interval between increased swimming speed and freezing
775 behavior for Cre- (75 ± 26.53 sec) and for Cre+ (20.88 ± 3.93 sec). For H-J, numbers represent the
776 mean ± SEM for n = 17 fish. *P < 0.05; **P < 0.01; ***P < 0.001; ****P < 0.0001; *n.s.*, not
777 significant (P > 0.05).
778

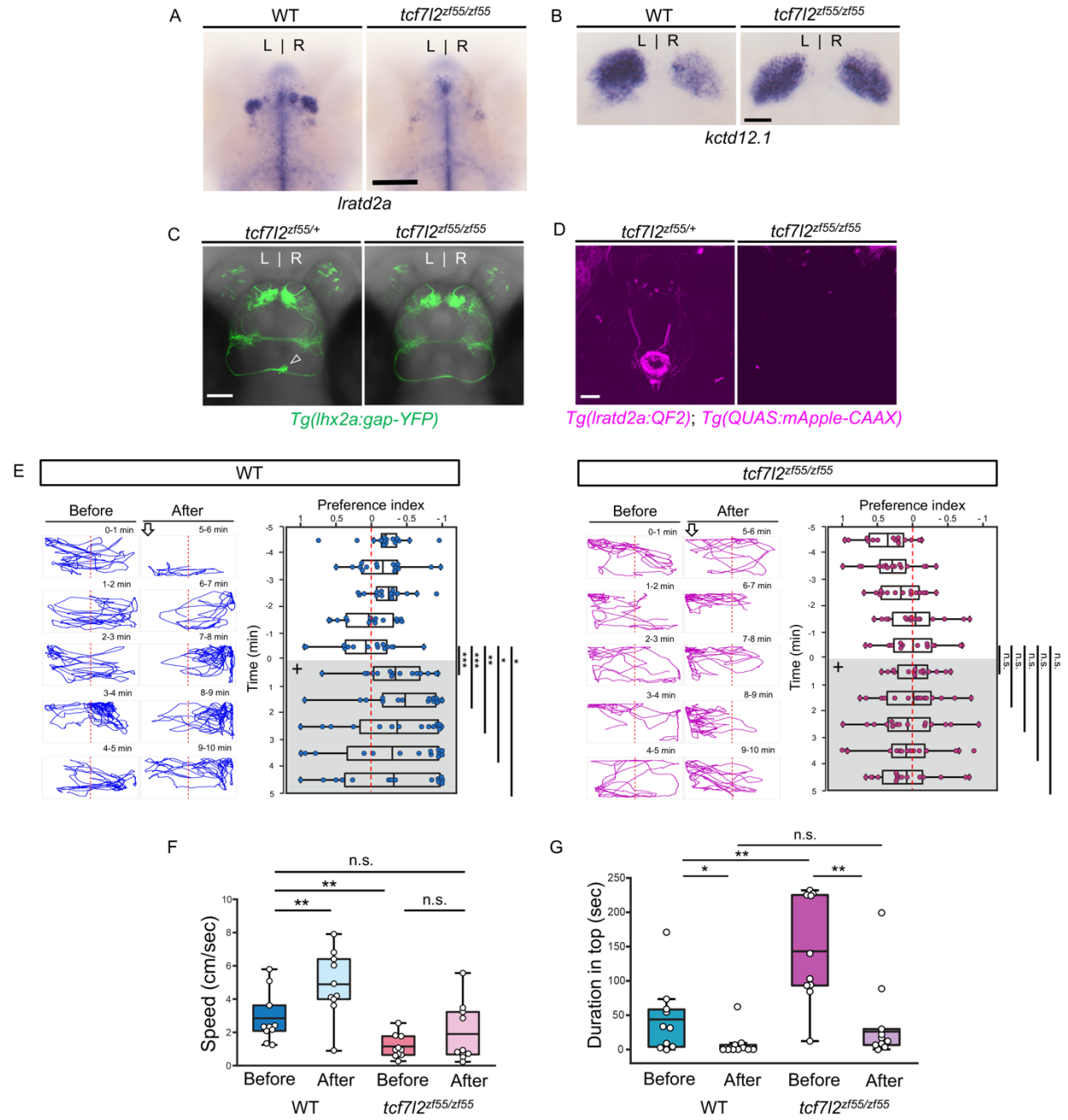

Figure 4. Attenuated response to aversive odorants in left-isomerized dHb mutants (A-B) (A) Absence of *lratd2a*-expressing right dHb neurons and (B) right-isomerized expression of *kctd12.1* in *tcf7l2* mutant larvae at 5 dpf. (C) Dorsal views of olfactory mitral neuronal projections of *Tg(lhx2a:gap-YFP)* larvae at 6 dpf. Open arrowhead indicates axon terminals of mitral cells in the WT right dHb that are absent in the mutant. (D) Dorsal views of dHb neuronal projections to

785 the ventral IPN in *Tg(lratd2a:QF2), Tg(QUAS:mApple-CAAX)* larvae at 6 dpf. (E) Representative
786 traces (1 min) and preference index for *tcf7l2* mutant and WT sibling adults after addition of
787 cadaverine (on + side). Only the WT siblings showed a significant difference in avoidance
788 behavior for the 5 mins afterwards compared to the min before its addition [6 min (P=0.00035), 7
789 min (P=0.000175), 8 min (P=0.0041), 9 min (P=0.0177), 10 min (P=0.0203), n = 15 adults.
790 Student's t-test]. (F) Swimming speed (cm/sec) for 30 sec before and after addition of alarm
791 substance. For *tcf7l2* homozygotes, 1.13 ± 0.22 cm/s and 1.89 ± 0.56 cm/s [Student's t test (P =
792 0.1011)] and for their WT siblings 2.84 ± 0.48 cm/s and 4.88 ± 0.63 cm/s [Student's t test
793 (P=0.0026)], n = 10 fish for each group (G) Duration in the upper half of the test tank prior to and
794 after addition of alarm substance for *tcf7l2* adults was 143.58 ± 24.80 sec and 38.77 ± 19.56 sec
795 (Mann-Whitney U=12; P=0.0047) and for their WT siblings was 43.68 ± 16.35 sec and 8.19 ± 6.16
796 sec (Mann-Whitney U=20.5, P=0.0285), n = 10 fish for each group. For F-G, numbers represent
797 the mean ± SEM. *$P < 0.05$; **$P < 0.01$; ***$P < 0.001$; *n.s.*, not significant (P > 0.05).
798

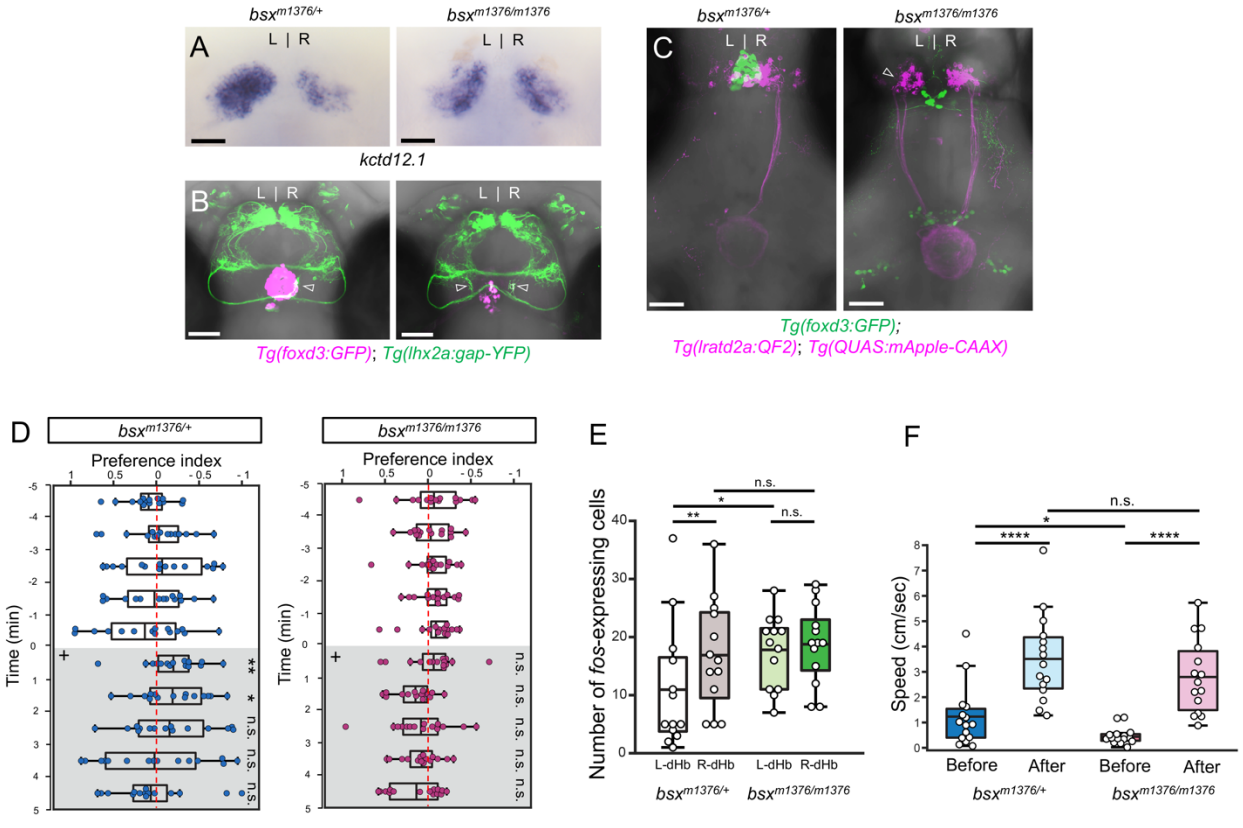

Figure 5. Enhanced reactivity to alarm substance in mutants with right-isomerized dHb

(A) Asymmetric expression of *kctd12.1* is right-isomerized in *bsx* homozygotes at 5 dpf. (B) Projections of *Tg(lhx2a:gap-YFP)* labeled olfactory mitral cells terminate bilaterally (open arrowheads) at *lratd2a* neurons in *bsx*^{m1376} homozygous mutants at 5 dpf. (C) In the mutants, axons from both left (open arrowhead) and right dHb *lratd2a* neurons project to the same region of the vIPN. Scale bar, 50 µm. (D) Preferred tank location of *bsx*^{m1376} adults after addition of cadaverine (on + side). Only the heterozygotes showed a significant difference in preference after application of cadaverine compared to the min before its addition [6 min (Mann-Whitney U = 37; P = 0.00188), 7 min (Mann-Whitney U = 56; P = 0.02034). n = 15 adults for each group]. (E) Quantification of *fos*-expressing cells in the dHb after application of cadaverine in *bsx*$^{m1376/+}$ [11 ± 2.97 cells on the left and 16.84 ± 2.62 cells on the right. Student's t-test (P=0.006)] and *bsx*$^{m1376/m1376}$ adults [17.61 ± 1.72 cells on the left and 18.77 ± 1.88 cells on the right. Student's t-

test (P=0.645)], for n = 13 sections from 7 adults for each group. (F) Swimming speed (cm/sec) for 30 sec before and after addition of alarm substance. In heterozygous adults, swimming speed was 1.22 ± 0.31 cm/s before and 3.52 ± 0.44 cm/s after [Student's t test (P=9.22089E-05)] and in homozygotes, 0.46 ± 0.08 cm/s before and 2.80 ± 0.37 cm/s after [Student's t test (P=1.38481E-05)], n = 15 adults for each group. For E-F, numbers represent the mean ± SEM. *P < 0.05; **P < 0.01; ****P < 0.0001; *n.s.*, not significant (P > 0.05).